Effects of Quantum and Dielectric Confinement on the Emission of Cs-Pb-Br Composites

Sebastián Caicedo-Dávila,* Pietro Caprioglio, Frederike Lehmann, Sergiu Levcenco, Martin Stolterfoht, Dieter Neher, Leeor Kronik, and Daniel Abou-Ras

The halide perovskite CsPbBr$_3$ belongs to the Cs-Pb-Br material system, which features two additional thermodynamically stable ternary phases, Cs$_4$PbBr$_6$ and CsPb$_2$Br$_5$. The coexistence of these phases and their reportedly similar photoluminescence (PL) have resulted in a debate on the nature of the emission in these systems. Herein, optical and microscopic characterizations are combined with an effective mass, correlated electron–hole model of excitons in confined systems, to investigate the emission properties of the ternary phases in the Cs-Pb-Br system. It is found that all Cs-Pb-Br phases exhibit green emission and the non-perovskite phases exhibit PL quantum yields orders of magnitude larger than CsPbBr$_3$. In particular, blue- and red-shifted emission for the Cs- and Pb-rich phases, respectively, are measured, stemming from embedded CsPbBr$_3$ nanocrystals (NCs). This model reveals that the difference in emission shift is caused by the combined effects of NC size and different band mismatch. Furthermore, the importance of including the dielectric mismatch in the calculation of the emission energy for Cs-Pb-Br composites is demonstrated. The results explain the reportedly limited blue shift in CsPbBr$_3$@Cs$_4$PbBr$_6$ composites and rationalize some of its differences with CsPb$_2$Br$_5$.

1. Introduction

The impressive progress in power conversion efficiency of solar cells based on halide perovskite-type (HaPs) compounds, from ≈4% in 2009[1] to more than 25% in recent years[2] has prompted significant research interest in these materials, not only for photovoltaics but also for other optoelectronic applications such as light emission and detection.[3–6] CsPbBr$_3$ is a prototypical model HaP,[7] which belongs to the Cs-Pb-Br material system with a great potential for applications in light-emitting diodes[8–14] and lasers.[15–17] Thus, understanding the emission properties of Cs-Pb-Br compounds is fundamental for the design of better materials and devices. The Cs-Pb-Br material system includes two additional, non-perovskite-type, ternary phases: The Cs-rich Cs$_4$PbBr$_6$ and the Pb-rich CsPb$_2$Br$_5$, sometimes referred to as the 0D and 2D phases, respectively, owing to their crystal structure (cf. Figure S1, Supporting Information). Both non-perovskite-type phases are thermodynamically stable and have been synthesized as single crystals, thin films, and nanocrystals (NCs).[18–23] The coexistence of Cs-Pb-Br phases and their influence on the optoelectronic properties are well established.[24-27] In recent years a strong green luminescence has been measured in both CsPb$_2$Br$_5$ and Cs$_4$PbBr$_6$, which appears to be in contrast with their large band-gap energies, ≈3.8 to 4 eV.[10,18,28-34] This motivated a debate on whether such luminescence is caused by intrinsic factors[35–43] or by NCs of the perovskite-type phase, CsPbBr$_3$

S. Caicedo-Dávila[+], F. Lehmann, S. Levcenco, D. Abou-Ras
Helmholtz-Zentrum Berlin für Materialien und Energien
Hahn-Meitner-Platz 1., 14109 Berlin, Germany
E-mail: sebastian.caicedo@tum.de

P. Caprioglio, M. Stolterfoht, D. Neher
Institute of Physics and Astronomy
University of Potsdam
14476 Potsdam, Germany

The ORCID identification number(s) for the author(s) of this article can be found under https://doi.org/10.1002/adfm.202305240

[+]Present address: Now at: Physics Department, TUM School of Natural Sciences, Technical University of Munich, James-Franck-Str. 1., 85748 Garching, Germany

P. Caprioglio
Clarendon Laboratory
Department of Physics
University of Oxford
Parks Road, Oxford OX1 3PU, UK

L. Kronik
Department of Molecular Chemistry and Materials Science
Weizmann Institute of Science
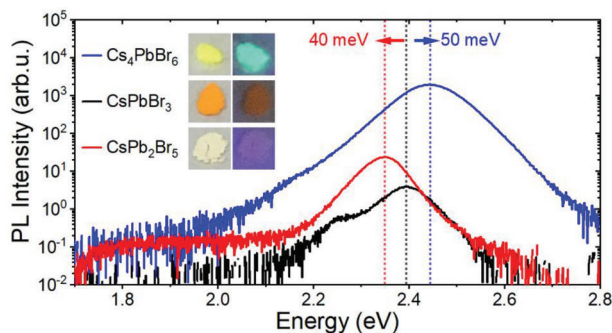Rehovoth 76100, Israel

**ADVANCED
SCIENCE NEWS**

www.advancedsciencenews.com

**ADVANCED
FUNCTIONAL
MATERIALS**

www.afm-journal.de

Figure 1. PL spectra of the three Cs-Pb-Br ternary phases. All the phases exhibit green luminescence between 2.3 and 2.5 eV. Spectra are plotted in a semi-logarithmic scale to show the differences in the PL intensity. Insets show photographs of the powder samples under ambient light (left) and 205 nm LED illumination (right).

(with band-gap energy in the green region of the visible spectrum, ≈ 2.4 eV),[7,42,44-54] embedded in the non-perovskite matrix. Although substantial evidence in favor of the embedded NCs hypothesis has been reported,[49,50,52-57] open questions remain, notably the exact mechanism that enhances the luminescence and the limited blue shift measured with decreasing NC size.[56]

In the present work, we combine photoluminescence (PL) and energy-dispersive X-ray (EDX) spectroscopies, as well as cathodoluminescence (CL) hyperspectral imaging and theoretical modeling to investigate the mechanisms behind the green emission in all three ternary phases of the Cs-Pb-Br material system. Our results provide additional evidence for the green emission in Cs_4PbBr_6 and $CsPb_2Br_5$ stemming from embedded $CsPbBr_3$ NCs. Furthermore, we model the exciton emission in $CsPbBr_3@Cs_4PbBr_6$ and $CsPbBr_3@CsPb_2Br_5$ composites using an effective mass model, which includes a simplified treatment of electron–hole correlation, as well as the band gap and dielectric mismatch at the interfaces. Comparing this model with the commonly used effective mass model[58,59] suggests that accounting for the effects of finite confinement potentials and the Coulomb interactions with image charges at the interface can result in better estimates of NC sizes. The model explains the limited blue shift in small $CsPbBr_3$ NCs embedded in Cs_4PbBr_6. Furthermore, differences in the type of confinement of $CsPbBr_3$ NCs in Cs_4PbBr_6 and $CsPb_2Br_5$ explain the stronger emission of the former case and the measured red shift of the latter case.

2. Results and Discussion

Powder samples of the Cs-Pb-Br ternary phases—$CsPbBr_3$, $CsPb_2Br_5$, and Cs_4PbBr_6—were synthesized as described in Section S1, Supporting Information. The three ternary phases exhibit PL emissions in the range from 2.3 to 2.5 eV, as shown in **Figure 1**. The integrated PL intensities of the $CsPb_2Br_5$ and Cs_4PbBr_6 are about one and three orders of magnitude larger, respectively, than that of the $CsPbBr_3$. Commensurately, the PL quantum yield (PLQY) at 1 sun equivalent illumination is $3 \times 10^{-3}\%$, 5%, and $8 \times 10^{-4}\%$ for $CsPb_2Br_5$, Cs_4PbBr_6, and $CsPbBr_3$, respectively. It is also noteworthy that the PL peak of green luminescence in the non-perovskite-type phases is shifted with respect to that of $CsPbBr_3$. A blue shift of 50 meV and a red

shift of 40 meV were measured for the PL peaks of Cs_4PbBr_6 and $CsPb_2Br_5$. The emission shifts are consistent among spectra measured on different sample areas and are significant, considering our measurement resolution (≈ 5 meV, see Section S2, Supporting Information) and the thermal energy at room temperature (≈ 25 meV).

We investigated the origin of the green emission in the $CsPb_2Br_5$ and Cs_4PbBr_6 samples using scanning electron microscopy (SEM), CL imaging, and EDX spectroscopy—see Figures **2–4** below. Experimental details are given in Section S2, Supporting Information. The CL maps for both Cs_4PbBr_6 and $CsPb_2Br_5$ show that luminescence in the visible spectral range stems from localized emitters, embedded in a solid matrix. Panchromatic (spectral range from 1.95 to 2.8 eV) and 500 nm bandpass-filtered maps are identical, confirming that the materials exhibit green emission (peak emission between 2.3 and 2.5 eV, cf. Figures 2 and 3). EDX elemental maps show that for Cs_4PbBr_6 the emitters exhibit higher Pb and lower Cs and Br counts (see Figure 2c–f), whereas for $CsPb_2Br_5$ the emitters exhibit lower Pb and higher Cs counts, but Br counts remain unchanged (cf. Figure 3c–e). The compositions of the emitting regions relative to the matrix suggest that they are $CsPbBr_3$. Therefore, we conclude that the green emitters are $CsPbBr_3$ NCs embedded in the host Cs_4PbBr_6 or $CsPb_2Br_5$ matrix.

In order to investigate the spectral features of the $CsPbBr_3$ NCs, we performed hyperspectral CL mapping, using a low acceleration voltage (3.5 kV) in order to avoid beam damage and reduce the interaction volume. This allows us to improve the spatial resolution of the CL signal around the NCs. The CL map of Cs_4PbBr_6 acquired at larger magnification shows that luminescence stems from clusters of NCs, rather than individual emitters (see Figure 4a). The NCs exhibit emission maxima in the range from 2.44 to 2.47 eV (spectrum 1 in Figure 4b), which agrees well with the PL measurement (cf. Figure 1). Furthermore, no emission was detected from the matrix material (spectrum 2 in Figure 4b). For the $CsPb_2Br_5$ sample, the CL spectra of the emitters peak between 2.35 and 2.37 eV (spectrum 1 in Figure 4e), in good agreement with the PL results (cf. Figure 1). The matrix material exhibits no sharp CL peak. However, we detected a wide band of weak emission centered at ≈ 1.9 eV (spectrum 2 in Figure 4e) when measuring CL on matrix regions. This observation is consistent with defect emission at the interface, we measured for $CsPb_2Br_5/CsPbBr_3$ films in previous work (cf. ref. [60] and its supplemental material).

Our CL-EDX correlative characterization clarifies the origin of the green emission in Cs_4PbBr_6 and $CsPb_2Br_5$. In order to understand the recombination mechanism and the nature of emission, we performed intensity-dependent PLQY measurements by exciting only the perovskite phase using a 445 nm laser (see **Figure 5**). Because of the excitation wavelength used, we can exclude charge transfer from the wide-gap, non-perovskite phases to the narrower perovskite ones. By investigating the slope γ of the dependence of the emitted photon flux ($I_{PL} = I^\gamma$) and the slope k of the dependence of the PLQY ($PLQY = I^k$) on the illumination intensity (I) in a log-log plot, it is possible to access charge recombination mechanisms. The green emission from the Cs_4PbBr_6 phase exhibits $\gamma = 1$ and $k \approx 0$. This indicates an excitonic character because it is known that a value of $\gamma = 1$ and intensity-independent PLQY correspond to the radiative
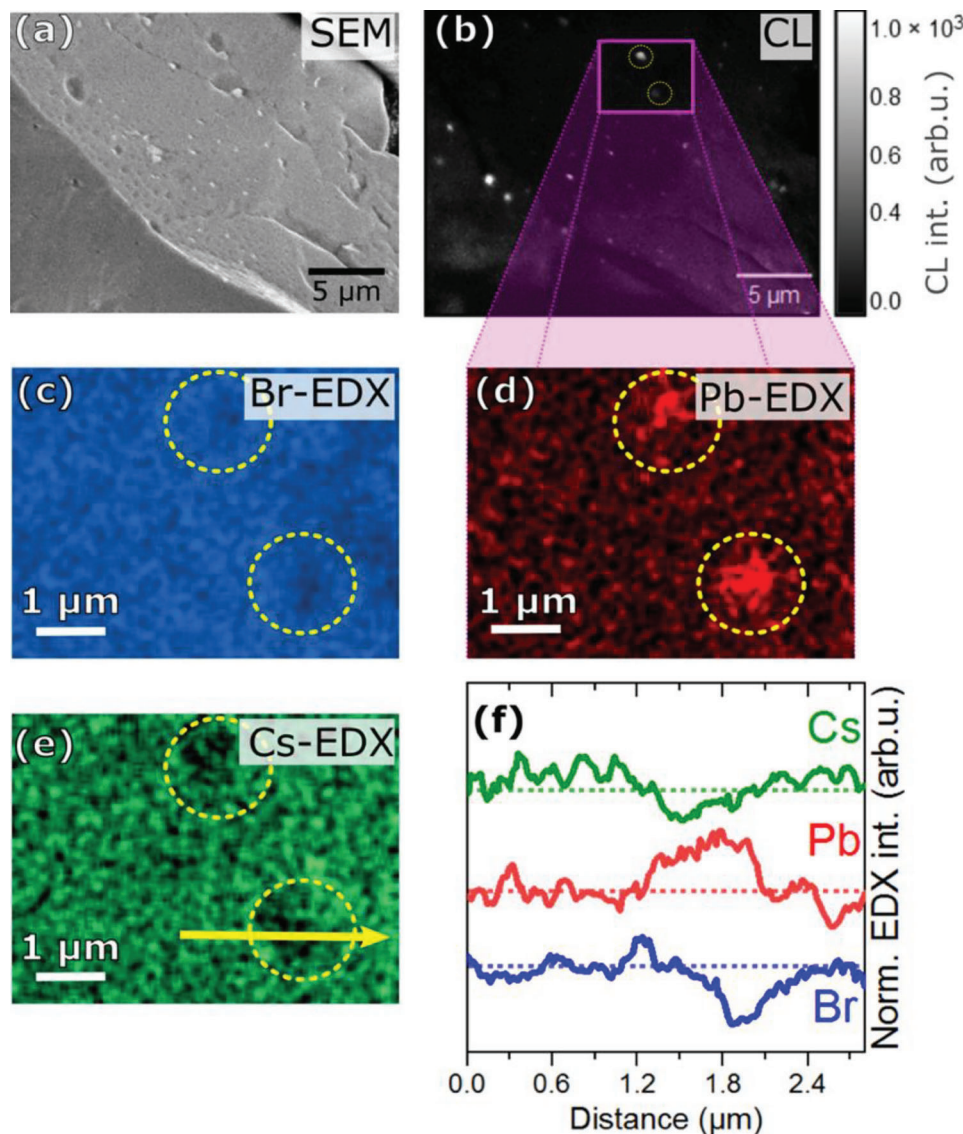
Figure 2. a) SEM image of Cs_4PbBr_6 crystal and b) a corresponding CL intensity map, filtered at 500 nm, showing the localized emitters embedded in the crystal. c–e) EDX elemental distribution maps and f) normalized line-scans—along the yellow arrow in (e)—of a magnified region, showing clear enrichment of Pb as well as depletion of Cs and Br, correlated with the yellow-circled position of highly luminescent clusters.

recombination of free excitons.[61–63] In contrast, the values of $\gamma = 1.5$ and $k = 0.5$ for $CsPb_2Br_5$ indicate a deviation from pure excitonic emission. This suggests that the green emission in this phase is dominated by nonradiative recombination. For the $CsPbBr_3$ phase, we find $\gamma = 1.1$ and $k = 0.1$, slightly deviating from a pure excitonic emission, and the absolute PLQY values are lower compared with those of Cs_4PbBr_6. This behavior suggests a stronger contribution of nonradiative recombination processes occurring in bulk $CsPbBr_3$, as compared with NC domains in Cs_4PbBr_6, suggesting that the latter is less defective. The contribution of nonradiative recombination processes can also be associated with the low PLQY of our Cs-Pb-Br composites, compared with the previous reports.[31,32,64]

The microscopy and spectroscopy results confirm consistently that the non-perovskite-type Cs-Pb-Br samples contain $CsPbBr_3$

NCs embedded in a solid matrix. The confinement of the NCs also explains the blue shift of the PL measured for Cs_4PbBr_6, with respect to bulk $CsPbBr_3$ emission (Figure 1). The best achievable spatial resolution for our CL experiments is in the range of $\approx$60–80 nm, as estimated from the density of Cs_4PbBr_6 (4.29 g cm^{-3})[65,66] and $CsPb_2Br_5$ (5.76 g cm^{-3}),[34,67] the electron beam parameters, and Gruen's equation (Equation (S1) in Section S2, Supporting Information). This resolution limit, as well as the diffusion of charge carriers before they recombine, limits the accuracy of the estimated NC size directly from CL experiments. Because the magnitude of quantum and dielectric confinement effects is generally related to the size of the NCs, it is interesting to examine whether a theoretical model can be used to provide an explanation for the origin of different blue- and red-shift effects and their dependence on the size of the emitting $CsPbBr_3$ NCs.
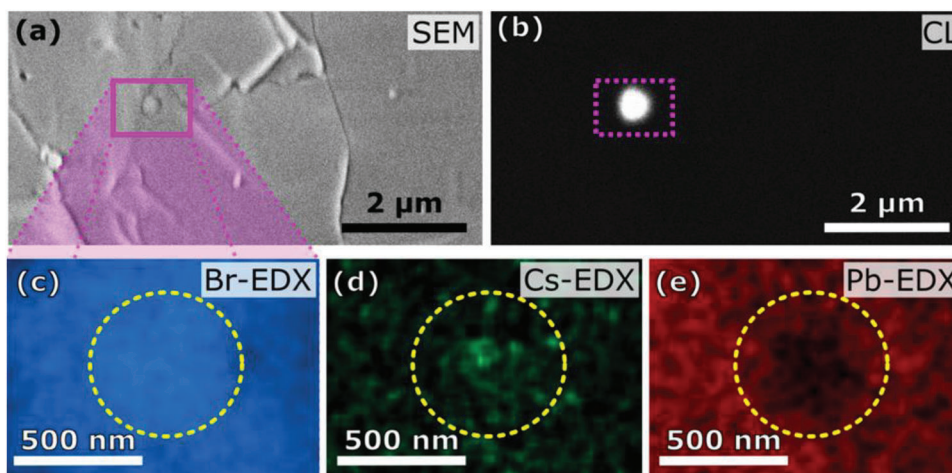
2305240 (3 of 9)

**ADVANCED
SCIENCE NEWS**

www.advancedsciencenews.com

**ADVANCED
FUNCTIONAL
MATERIALS**

www.afm-journal.de

Figure 3. a) SEM image of a $CsPb_2Br_5$ crystal and b) a corresponding CL intensity map, filtered at 500 nm. EDX elemental distribution maps of c) Br, d) Cs, and e) Pb show a clear enrichment of Cs and depletion of Pb, correlated with the yellow-circled position of highly luminescent clusters.

An important and commonly used approximation to the emission in such systems, within the effective mass approximation, has been proposed by Brus in the 80s.[58,59,68] This model considers a spherical NC in an infinite potential well, where the Coulomb interaction is strongly screened, such that the exciton (electron–hole) wave function is uncorrelated. However, as stated by Brus in his original paper,[58] this model can be a poor approximation for large band gap materials with moderate NC sizes because in those systems the Coulomb energy is comparable to the confinement energy, and the electron–hole correlation can be important. Considering that $CsPbBr_3$ is indeed a (relatively) large gap material with a (relatively) significant exciton binding energy (35–60 meV),[39,69–72] we opt for a simple model, enforcing confinement in one dimension, that includes some form of electron–hole correlation, while remaining mathematically tractable and computationally inexpensive. We show below that this is sufficient for a qualitative explanation of our results.

We apply an effective mass model, proposed by Rajadell et al. for CdSe nanostructures,[73–77] The model explicitly treats the correlated electron–hole pair, including Coulomb interactions and dielectric effects, based on the method of image charges that approximate polarization terms in the exciton Hamiltonian (see Section S3, Supporting Information, for further details). Within this framework, the Hamiltonian that describes the electron–hole pair is given by

$$H\left(r_e, r_h\right) = H^{(e)}\left(r_e\right) + H^{(h)}\left(r_h\right) + V_c\left(r_e, r_h\right) \tag{1}$$

where $H^{(i)}(r_i)$ is an effective-mass, single-particle Hamiltonian, that contains image charge effects, which is described in detail in Equation (S2), Supporting Information. $V_c(r_e, r_h)$ is a generalized electron–hole Coulomb interaction potential, calculated using the method of image charges. This term describes the interaction of a charged particle with interface image
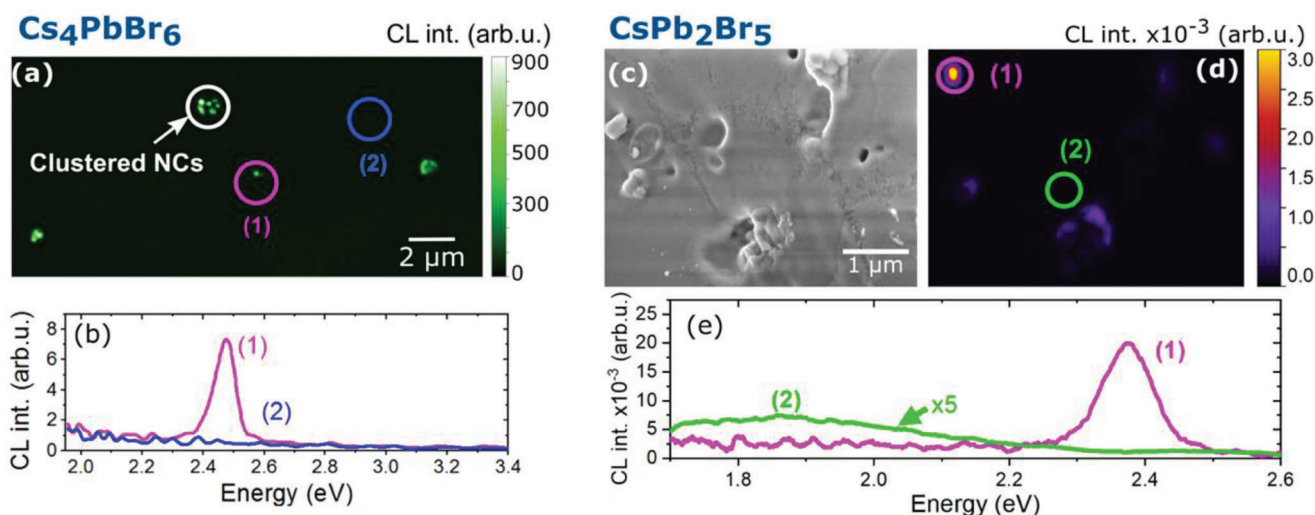

Figure 4. a) CL intensity map, filtered at 500 nm, on a flat surface of a Cs_4PbBr_6 crystal. b) Corresponding CL spectra (hyperspectral measurement without filter) of selected areas. c) SEM image of the surface of $CsPb_2Br_5$. d) Corresponding CL map, filtered at 550 nm, and e) CL spectra of selected areas. Spectrum 2 is magnified ×5 for visibility.

**ADVANCED
SCIENCE NEWS**

www.advancedsciencenews.com

**ADVANCED
FUNCTIONAL
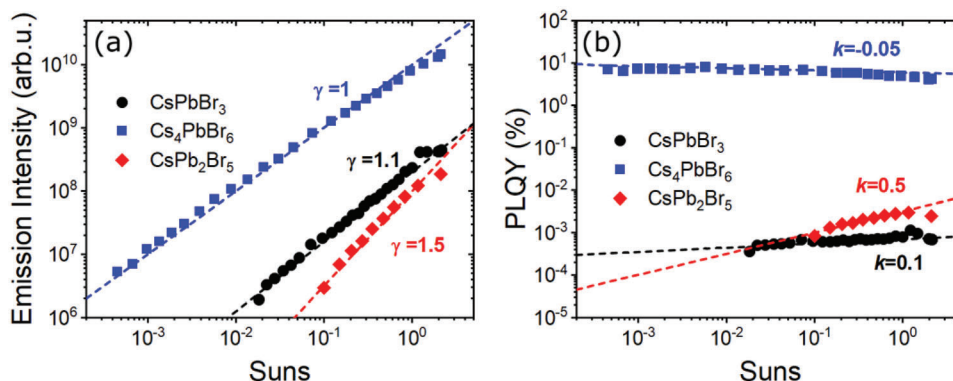MATERIALS**

www.afm-journal.de

Figure 5. a) PL emitted photon flux and b) PLQY as a function of the excitation intensity. The data are plotted in a logarithmic scale and linearly fit. The slope of the PL (γ) and PLQY (k) curves reveals the type of dominant recombination, see text for details.

charges induced by the other particle and can be written in one dimension as[77]

$$V_c\left(r_e, r_h\right) = \sum_{n=-\infty}^{\infty} \frac{q_n e^2}{\epsilon_1 \sqrt{\left\|r_{\parallel,e} - r_{\parallel,h}\right\|^2 + \left[z_e - (-1)^n z_h + nL\right]^2}} \quad (2)$$

where $r_{\parallel,i}$ is the in-plane particle position (perpendicular to the confinement direction), z_i is the particle position in the confined direction, L is the width of the well (NC size), and $q_n = \left(\frac{\epsilon_1 - \epsilon_2}{\epsilon_1 + \epsilon_2}\right)^{|n|}$, where ϵ_1 and ϵ_2 are the dielectric constant of the NC and host, respectively. We seek a two-particle wave-function solution to this Hamiltonian, namely

$$H\left(r_e, r_h\right) \Psi\left(r_e, r_h\right) = E_{exc} \Psi\left(r_e, r_h\right) \quad (3)$$

where the wave function is approximated by[76]

$$\Psi\left(r_e, r_h\right) = N\psi_e\left(r_e\right) \psi_h\left(r_h\right) e^{-a\sqrt{\left\|r_{\parallel,e} - r_{\parallel,h}\right\|^2}} \quad (4)$$

where $\psi_{e/h}$ are the single-particle wave functions for electron and hole, and a is a variational parameter. Solving Equations (1)–(4) requires electron and hole effective masses, as well as dielectric constant values. For the former, we use the values reported by Protesescu et al.[71] for $CsPbBr_3$. For the latter, we used density functional perturbation theory (DFPT) to obtain computed values for all three Cs-Pb-Br phases (see Section S4, Supporting Information, for details). All parameters used in the model are summarized in Table S1, Supporting Information.

When $\epsilon_1 > \epsilon_2$, that is, the dielectric constant of the NC is larger than that of the host, there is dielectric confinement. The image charge induced at the interface exhibits the same sign as the confined charge and the electric field owing to the confined charge penetrates the matrix region, as shown schematically in **Figure 6**a. This reduces the effective dielectric constant, with respect to ϵ_1, and enhances the Coulomb interaction between electron and hole.[73,78] The electron–hole Coulomb interaction is further modulated by the overlap between the electron and hole wave functions, which depends on the degree of confinement. Consequently, the exciton binding energy will be a function not only of ϵ_1 and ϵ_2, but also of the NC size.

We first use the above model to investigate the effect of a dielectric mismatch for an NC confined by an infinite potential. We calculate the shift of the emission energy, E_{em} with respect to the bulk band gap of $CsPbBr_3$, E_g, as a function of the NC size L, for various values of ϵ_2 (see Figure 6b). For small L, quantum confinement is dominant, and the effect of dielectric mismatch on $E_{em} - E_g$ is negligible. As L increases and quantum confinement is reduced, the effect of dielectric mismatch becomes more important, and $E_{em} - E_g$ decreases with ϵ_2 owing to a stronger dielectric confinement. Dielectric effects also directly impact the exciton binding energy, E_b, namely the difference between the emission energy and the single-particle bandgap, as shown in Figure 6c,d. Because dielectric confinement reduces the effective dielectric constant and Coulomb screening, it increases E_b. Specifically, E_b rapidly decreases with L for $\epsilon_2 < \epsilon_1$. This dependence weakens as ϵ_2 increases, demonstrating that dielectric confinement is stronger for smaller NCs, in good agreement with previous reports.[73,77,79–81]

Next, we investigate the effect of a finite confinement potential on the emission energy, by including the band mismatch between NC and matrix material, that is, Cs_4PbBr_6 or $CsPb_2Br_5$ (see Section S3, Supporting Information, for details). We use the literature-reported band-gap energies of the Cs-Pb-Br phases, that is, 2.4 eV for $CsPbBr_3$ (in reasonable agreement with our measurements),[7,44–48] 4 eV for Cs_4PbBr_6,[28–32] and 3.7 eV for $CsPb_2Br_5$.[18,33,34] The band mismatch for $CsPbBr_3/Cs_4PbBr_6$ results in a type I band alignment, that is, both hole and electron wave functions are confined, as deduced from both theoretical calculations[82] and (X-ray and UV) photoelectron spectroscopy.[83,84] We model the type I alignment using a fixed band mismatch $\frac{\Delta E_g}{2}$ (where $\Delta E_g = E_g^{Cs_4PbBr_6} - E_g^{CsPbBr_3}$) for the conduction and valence band mismatch. In the case of $CsPbBr_3/CsPb_2Br_5$, some theory reports a quasi-type I alignment (only one carrier confined),[85] while experimental characterization assigns a type II band alignment,[86] that is, the electrons and holes are confined to different regions, which reduces their wave function overlap. We modeled this by setting a small but negative valence band offset $\Delta E_V = -0.1$ eV and a corresponding conductions band offset of $\Delta E_C = \Delta E_g + 0.1$ eV (where $\Delta E_g = E_g^{CsPb_2Br_5} - E_g^{CsPbBr_3}$).

The effect of the finite band mismatch is apparent in the calculated shift in emission energy $E_{em} - E_g$, shown in **Figure 7**,
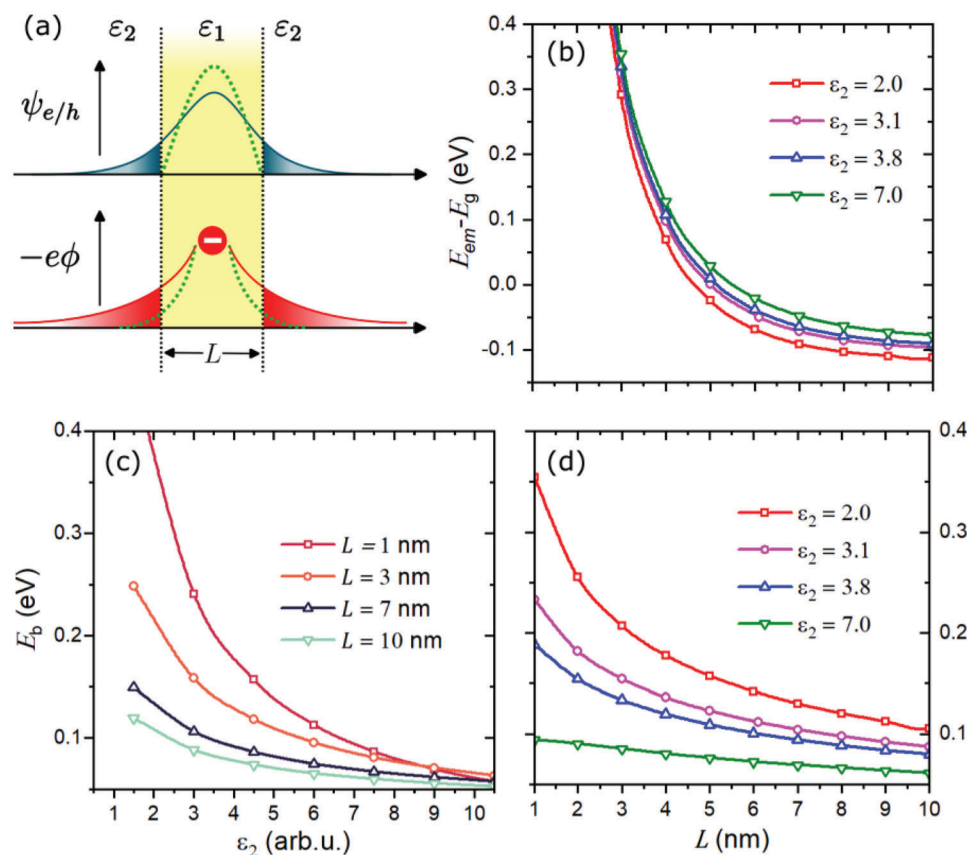
2305240 (5 of 9)

ADVANCED
SCIENCE NEWS
www.advancedsciencenews.com

ADVANCED
FUNCTIONAL
MATERIALS
www.afm-journal.de

Figure 6. Effect of confinement and dielectric mismatch in a simple 1D model of a CsPbBr$_3$ NC. a) Top: schematic representation of a single-particle wave function, $\psi_{e/h}$, confined in an infinite (dashed) and finite (solid) potential. Bottom: schematic representation of the effect of dielectric mismatch on the electrostatic potential, ϕ, for $\epsilon_1 > \epsilon_2$ (solid) and $\epsilon_1 < \epsilon_2$ (dashed). b) Calculated shift of the emission energy with respect to the bulk band gap energy, $E_{em} - E_g$, as a function of the NC size for different values of ϵ_2. c) Exciton binding energy, E_b, as a function of ϵ_2 for various NC sizes. d) E_b as a function of **L** for various ϵ_2.

where the finite potential reduces the magnitude of the quantum confinement effect. This effect is stronger in Cs$_4$PbBr$_6$ than it is in CsPb$_2$Br$_5$, partly because of the larger band gap of the former, but mostly due to the more effective quantum confinement of the type I alignment. Generally, for a finite confinement

potential the wave function extends into the barrier regions (cf. Figure 6a), making quantum confinement less effective and also reducing the effective dielectric constant of the system, thereby favoring dielectric confinement.[73] At the same time, the decrease in electron–hole overlap reduces the Coulomb interaction,
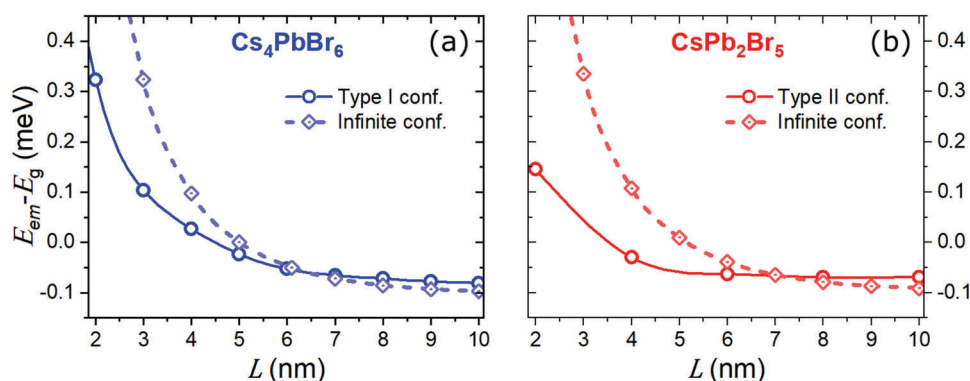

Figure 7. Emission energy shift, $E_{em} - E_g$, of a CsPbBr$_3$ NC embedded in a) Cs$_4$PbBr$_6$, or b) CsPb$_2$Br$_5$, as a function of the NC size. A dielectric mismatch is modeled with $\epsilon_1 = 4.2$ for CsPbBr$_3$, $\epsilon_2 = 3.1$ for Cs$_4$PbBr$_6$, and $\epsilon_2 = 3.8$ for CsPb$_2$Br$_5$. Results for infinite (dashed curves) and finite (solid curves) confinement potentials, with type I and type II alignments for Cs$_4$PbBr$_6$ and CsPb$_2$Br$_5$, respectively, are compared.

**ADVANCED
SCIENCE NEWS**

www.advancedsciencenews.com

**ADVANCED
FUNCTIONAL
MATERIALS**

www.afm-journal.de

hindering dielectric confinement. This competition results in a complex dependence of the exciton binding energy on the finite potential barriers. In the present calculation, confinement effects are apparent for $L < 6.3$ nm (<7 nm) for Cs_4PbBr_6 ($CsPb_2Br_5$), providing a guide to the size regimes for which quantum or dielectric confinement is dominant. While the similarity to the exciton Bohr radius of bulk $CsPbBr_3$ (≈ 7 nm)[71] is notable, we emphasize that this is a 1D model, which should not be compared fully quantitatively to the experiment.

We can now qualitatively interpret our experimental data, in light of the computed result from the above model. In the case of Cs_4PbBr_6, it is clear that the size of the embedded $CsPbBr_3$ NCs lies in the strong confinement regime, that is, quantum confinement is dominant and results in the above-reported blue shift and PLQY enhancement of the exciton emission. The blue shift in this system is reduced with respect to the conventional estimations using a simple effective mass model, owing to the combined effect of a finite confinement potential and the reduced effective dielectric constant. This rationalizes the limited emission shift achieved experimentally for $CsPbBr_3@Cs_4PbBr_6$ composites.[32,56] For $CsPb_2Br_5$, a plausible explanation for the red shift measured in our PL and CL experiments is that there is weaker quantum confinement caused by type II band alignment, coupled with larger NC sizes, expected from the similar formation enthalpies of the $CsPbBr_3$ and $CsPb_2Br_5$ phases.[26,27,60] For larger NCs, the dielectric mismatch can cause enough of an increase in the exciton binding energy to overcome the effect of the weak quantum confinement, resulting in a net red shift in E_{em} with respect to the bulk E_g. This also can explain the large discrepancy between NC sizes estimated with a simple effective mass model and the TEM images, reported for $CsPb_2Br_5$. For this case, the error in the estimation of the NC size was found to be as large as 4 nm, which is much larger than the error for Cs_4PbBr_6 (0.6 nm).[87]

While the simple model provides a plausible qualitative explanation for all emission energy patterns observed in our experiments, we caution that further refinement is needed to gain a complete quantitative understanding of the PL results from the composite Cs-Pb-Br materials. First, the model used in the present work is 1D, whereas the effects of dielectric and quantum confinement could be stronger and have a more complex relationship in a system confined in all three spatial dimensions. For example, the dielectric tensor of $CsPb_2Br_5$ is highly anisotropic, that is, the effect of dielectric mismatch would depend strongly on the confinement direction. Also, in our model, we did not consider changes in the electron and hole effective masses, which can also influence the exciton levels.[68,88] Furthermore, considering the exciton fine structure of the $CsPbBr_3$ NCs, including effective mass non-parabolicity using an energy-dependent effective mass, as described by Sercel et al.,[89,90] will help improve the accuracy of the model, making it more comparable with experimental results. Ghribi et al. recently used similar models, combined with exciton fine structure to study dielectric confinement in $CsPbBr_3$ NCs.[91] Our results on the dielectric tensor, band alignment, and finite confinement effect of the NCs in Cs_4PbBr_6 and $CsPb_2Br_5$ could contribute to refining this model, explain experimental results, and provide material design guidelines for Cs-Pb-Br composites. Additionally, this work could be extended to study other halide composites such as Cs_4PbCl_6 and Cs_4PbI_6.

These compounds have also been shown to coexist with their corresponding perovskite phases.[92-94] The change in the halide offers an additional degree of freedom (i.e., composition) for tuning the exciton emission in Cs-Pb-X (X = Br, Cl, I) composites.

3. Conclusions

In summary, we synthesized green-luminescent, ternary phases in the Cs-Pb-Br material system, namely perovskite-type $CsPbBr_3$ and non-perovskite-types Cs_4PbBr_6 and $CsPb_2Br_5$. We investigated their emission properties using PL experiments, which showed that the non-perovskite-type phases exhibit a higher quantum yield, with a blue shift of 50 meV and a red shift of 40 meV (with respect to the PL peak of bulk $CsPbBr_3$) for the Cs_4PbBr_6 and $CsPb_2Br_5$ phases, respectively. Microscopic characterization by means of correlative CL hyperspectral imaging, as well as EDX elemental mapping, showed that the luminescence emission at 2.45 and 2.36 eV of Cs_4PbBr_6 and $CsPb_2Br_5$ stems from NCs of $CsPbBr_3$, embedded in the matrix material. We qualitatively explained the experimental results using a 1D effective-mass model that considers electron–hole correlation, as well as band gap and dielectric mismatch at the interface of the NC and host materials. This model allowed us to rationalize the effect of the quantum and dielectric confinements on the emission shifts. We showed that including dielectric effects is important for estimating the emission energy and particle size. In the light of the correlated model, we conclude that the $CsPbBr_3@Cs_4PbBr_6$ composite is formed by small, strongly quantum-confined $CsPbBr_3$ NCs in a Cs_4PbBr_6 matrix, while the $CsPbBr_3@CsPb_2Br_5$ composite is formed by large and weakly confined $CsPbBr_3$ NCs in a $CsPb_2Br_5$ matrix, in which dielectric effects dominate, resulting in a net red shift.

Supporting Information

Supporting Information is available from the Wiley Online Library or from the author.

Conflict of Interest

The authors declare no conflict of interest.

Data Availability Statement

The data that support the findings of this study are available from the corresponding author upon reasonable request.

**ADVANCED
SCIENCE NEWS**

www.advancedsciencenews.com

**ADVANCED
FUNCTIONAL
MATERIALS**

www.afm-journal.de

[1] A. Kojima, K. Teshima, Y. Shirai, T. Miyasaka, *J. Am. Chem. Soc.* **2009**, *131*, 6050.

[2] M. A. Green, E. D. Dunlop, J. Hohl-Ebinger, M. Yoshita, N. Kopidakis, X. Hao, *Prog. Photovoltaics* **2021**, *29*, 657.

[3] S. D. Stranks, H. J. Snaith, *Nat. Nanotechnol.* **2015**, *10*, 391.

[4] T. M. Brenner, D. A. Egger, L. Kronik, G. Hodes, D. Cahen, *Nat. Rev. Mater.* **2016**, *1*, 15007.

[5] M. Ahmadi, T. Wu, B. Hu, *Adv. Mater.* **2017**, *29*, 1605242.

[6] Q. Van Le, H. W. Jang, S. Y. Kim, *Small Methods* **2018**, *2*, 1700419.

[7] M. Kulbak, D. Cahen, G. Hodes, *J. Phys. Chem. Lett.* **2015**, *6*, 2452.

[8] N. Yantara, S. Bhaumik, F. Yan, D. Sabba, H. A. Dewi, N. Mathews, P. P. Boix, H. V. Demir, S. Mhaisalkar, *J. Phys. Chem. Lett.* **2015**, *6*, 4360.

[9] X. Zhang, B. Xu, J. Zhang, Y. Gao, Y. Zheng, K. Wang, X. W. Sun, *Adv. Funct. Mater.* **2016**, *26*, 4595.

[10] C. Qin, T. Matsushima, A. S. D. Sandanayaka, Y. Tsuchiya, C. Adachi, *J. Phys. Chem. Lett.* **2017**, *8*, 5415.

[11] Y. M. Chen, Y. Zhou, Q. Zhao, J. Y. Zhang, J. P. Ma, T. T. Xuan, S. Q. Guo, Z. J. Yong, J. Wang, Y. Kuroiwa, C. Moriyoshi, H. T. Sun, *ACS Appl. Mater. Interfaces* **2018**, *10*, 15905.

[12] K. Lin, J. Xing, L. N. Quan, F. P. G. de Arquer, X. Gong, J. Lu, L. Xie, W. Zhao, D. Zhang, C. Yan, W. Li, X. Liu, Y. Lu, J. Kirman, E. H. Sargent, Q. Xiong, Z. Wei, *Nature* **2018**, *562*, 245.

[13] Y. F. Ng, N. F. Jamaludin, N. Yantara, M. Li, V. K. R. Irukuvarjula, H. V. Demir, T. C. Sum, S. Mhaisalkar, N. Mathews, *ACS Omega* **2017**, *2*, 2757.

[14] X. Li, Z. Wen, S. Ding, F. Fang, B. Xu, J. Sun, C. Liu, K. Wang, X. W. Sun, *Adv. Opt. Mater.* **2020**, *8*, 2000232.

[15] X. Tang, Z. Hu, W. Yuan, W. Hu, H. Shao, D. Han, J. Zheng, J. Hao, Z. Zang, J. Du, Y. Leng, L. Fang, M. Zhou, *Adv. Opt. Mater.* **2017**, *5*, 1600788.

[16] N. Pourdavoud, T. Haeger, A. Mayer, P. J. Cegielski, A. L. Giesecke, R. Heiderhoff, S. Olthof, S. Zaefferer, I. Shutsko, A. Henkel, D. Becker-Koch, M. Stein, M. Cehovski, O. Charfi, H. Johannes, D. Rogalla, M. C. Lemme, M. Koch, Y. Vaynzof, K. Meerholz, W. Kowalsky, H. Scheer, P. Görrn, T. Riedl, *Adv. Mater.* **2019**, *31*, 1903717.

[17] Y. Mao, C. Liang, G. Wang, Y. Wang, Z. Zhang, B. Wang, Z. Wen, Z. Mu, G. Sun, S. Chen, G. Xing, *Adv. Opt. Mater.* **2022**, *10*, 2201845.

[18] I. Dursun, M. De Bastiani, B. Turedi, B. Alamer, A. Shkurenko, J. Yin, A. M. El-Zohry, I. Gereige, A. AlSaggaf, O. F. Mohammed, M. Eddaoudi, O. M. Bakr, *ChemSusChem* **2017**, *10*, 3746.

[19] F. Palazon, C. Urso, L. De Trizio, Q. Akkerman, S. Marras, F. Locardi, I. Nelli, M. Ferretti, M. Prato, L. Manna, *ACS Energy Lett.* **2017**, *2*, 2445.

[20] F. Palazon, S. Dogan, S. Marras, F. Locardi, I. Nelli, P. Rastogi, M. Ferretti, M. Prato, R. Krahne, L. Manna, *J. Phys. Chem. C* **2017**, *121*, 11956.

[21] Q. A. Akkerman, S. Park, E. Radicchi, F. Nunzi, E. Mosconi, F. De Angelis, R. Brescia, P. Rastogi, M. Prato, L. Manna, *Nano Lett.* **2017**, *17*, 1924.

[22] M. Liu, J. Zhao, Z. Luo, Z. Sun, N. Pan, H. Ding, X. Wang, *Chem. Mater.* **2018**, *30*, 5846.

[23] S. K. Balakrishnan, P. V. Kamat, *Chem. Mater.* **2018**, *30*, 74.

[24] G. Maity, S. K. Pradhan, *J. Alloys Compd.* **2020**, *816*, 152612.

[25] B. Turedi, K. J. Lee, I. Dursun, B. Alamer, Z. Wu, E. Alarousu, O. F. Mohammed, N. Cho, O. M. Bakr, *J. Phys. Chem. C* **2018**, *122*, 14128.

[26] S. Caicedo-Dávila, H. Funk, R. Lovrincic, C. Müller, C. Müller, M. Sendner, O. Cojocaru-Mirédin, F. Lehmann, R. Gunder, A. Franz, S. Levcenko, S. Levcenco, A. V. Cohen, L. Kronik, B. Haas, B. Haas, C. Koch, D. Abou-Ras, *J. Phys. Chem. C* **2019**, *123*, 17666.

[27] Z.-L. Yu, Y.-Q. Zhao, Q. Wan, B. Liu, J.-L. Yang, M.-Q. Cai, *J. Phys. Chem. C* **2020**, *124*, 23052.

[28] M. Nikl, E. Mihokova, K. Nitsch, F. Somma, C. Giampaolo, G. P. Pazzi, P. Fabeni, S. Zazubovich, *Chem. Phys. Lett.* **1999**, *306*, 280.

[29] V. Babin, P. Fabeni, E. Mihokova, M. Nikl, G. P. Pazzi, *Phys. Status Solidi B* **2000**, *205*, 205.

[30] C. D. Weerd, J. Lin, L. Gomez, Y. Fujiwara, K. Suenaga, T. Gregorkiewicz, *J. Phys. Chem. C* **2017**, *121*, 19490.

[31] L. N. Quan, R. Quintero-Bermudez, O. Voznyy, G. Walters, A. Jain, J. Z. Fan, X. Zheng, Z. Yang, E. H. Sargent, *Adv. Mater.* **2017**, *29*, 1605945.

[32] X. Chen, F. Zhang, Y. Ge, L. Shi, S. Huang, J. Tang, Z. Lv, L. Zhang, B. Zou, H. Zhong, *Adv. Funct. Mater.* **2018**, *28*, 1706567.

[33] Z. Zhang, Y. Zhu, W. Wang, W. Zheng, R. Lin, F. Huang, *J. Mater. Chem. C* **2018**, *6*, 446.

[34] O. Nazarenko, M. R. Kotyrba, M. Wörle, E. Cuervo-Reyes, S. Yakunin, M. V. Kovalenko, *Inorg. Chem.* **2017**, *56*, 11552.

[35] M. I. Saidaminov, J. Almutlaq, S. Sarmah, I. Dursun, A. A. Zhumekenov, R. Begum, J. Pan, N. Cho, O. F. Mohammed, O. M. Bakr, *ACS Energy Lett.* **2016**, *1*, 840.

[36] J. Yin, Y. Zhang, A. Bruno, C. Soci, O. M. Bakr, J. L. Brédas, O. F. Mohammed, *ACS Energy Lett.* **2017**, *2*, 2805.

[37] S. Seth, A. Samanta, *J. Phys. Chem. Lett.* **2017**, *8*, 4461.

[38] M. De Bastiani, I. Dursun, Y. Zhang, B. A. Alshankiti, X. H. Miao, J. Yin, E. Yengel, E. Alarousu, B. Turedi, J. M. Almutlaq, M. I. Saidaminov, S. Mitra, I. Gereige, A. Alsaggaf, Y. Zhu, Y. Han, I. S. Roqan, J. L. Bredas, O. F. Mohammed, O. M. Bakr, *Chem. Mater.* **2017**, *29*, 7108.

[39] J.-H. H. Cha, J. H. Han, W. Yin, C. Park, Y. Park, T. K. Ahn, J. H. Cho, D.-Y. Y. Jung, *J. Phys. Chem. Lett.* **2017**, *8*, 565.

[40] J. Yin, H. Yang, K. Song, A. M. El-Zohry, Y. Han, O. M. Bakr, J. L. Brédas, O. F. Mohammed, *J. Phys. Chem. Lett.* **2018**, *9*, 5490.

[41] Y. K. Jung, J. Calbo, J. S. Park, L. D. Whalley, S. Kim, A. Walsh, *J. Mater. Chem. A* **2019**, *7*, 20254.

[42] T. Zhang, Z. Chen, Y. Shi, Q. H. Xu, *Nanoscale* **2019**, *11*, 3216.

[43] P. Acharyya, P. Pal, P. K. Samanta, A. Sarkar, S. K. Pati, K. Biswas, *Nanoscale* **2019**, *11*, 4001.

[44] K. Nitsch, V. Hamplová, M. Nikl, K. Polák, M. Rodová, *Chem. Phys. Lett.* **1996**, *258*, 518.

[45] Y. Rakita, N. Kedem, S. Gupta, A. Sadhanala, V. Kalchenko, M. L. Böhm, M. Kulbak, R. H. Friend, D. Cahen, G. Hodes, *Cryst. Growth Des.* **2016**, *16*, 5717.

[46] Q. A. Akkerman, S. G. Motti, A. R. S. Kandada, E. Mosconi, V. D'Innocenzo, G. Bertoni, S. Marras, B. A. Kamino, L. Miranda, F. De Angelis, A. Petrozza, M. Prato, L. Manna, *J. Am. Chem. Soc.* **2016**, *138*, 1010.

[47] J. Liang, J. Liu, Z. Jin, *Sol. RRL* **2017**, *1*, 1770138.

[48] J. Lei, F. Gao, H. Wang, J. Li, J. Jiang, X. Wu, R. Gao, Z. Yang, S. Frank Liu, *Sol. Energy Mater. Sol. Cells* **2018**, *187*, 1.

[49] Z. Qin, S. Dai, V. G. Hadjiev, C. Wang, L. Xie, Y. Ni, C. Wu, G. Yang, S. Chen, L. Deng, Q. Yu, G. Feng, Z. M. Wang, J. Bao, *Chem. Mater.* **2019**, *31*, 9098.

[50] N. Riesen, M. Lockrey, K. Badek, H. Riesen, *Nanoscale* **2019**, *11*, 3925.

[51] M. Shin, S.-W. Nam, A. Sadhanala, R. Shivanna, M. Anaya, A. Jiménez-Solano, H. Yoon, S. Jeon, S. D. Stranks, R. L. Z. Hoye, B. Shin, *ACS Appl. Energy Mater.* **2020**, *3*, 192.

[52] Z. Ma, F. Li, D. Zhao, G. Xiao, B. Zou, *CCS Chem.* **2020**, *2*, 71.

[53] S. Aharon, L. Etgar, *Nano Select* **2021**, *2*, 83.

[54] W. Castro Ferreira, B. S. Araújo, M. A. P. Gómez, F. E. O. Medeiros, C. W. de Araujo Paschoal, C. B. da Silva, P. T. C. Freire, U. F. Kaneko, F. M. Ardito, N. M. Souza-Neto, A. P. Ayala, *J. Phys. Chem. C* **2022**, *126*, 541.

[55] J. Xu, W. Huang, P. Li, D. R. Onken, C. Dun, Y. Guo, K. B. Ucer, C. Lu, H. Wang, S. M. Geyer, R. T. Williams, D. L. Carroll, *Adv. Mater.* **2017**, *29*, 1703703.

[56] Q. A. Akkerman, A. L. Abdelhady, L. Manna, *J. Phys. Chem. Lett.* **2018**, *9*, 2326.

[57] U. Petralanda, G. Biffi, S. C. Boehme, D. Baranov, R. Krahne, L. Manna, I. Infante, *Nano Lett.* **2021**, *21*, 8619.

[58] L. E. Brus, *J. Chem. Phys.* **1984**, *80*, 4403.

[59] L. Brus, *J. Phys. Chem.* **1986**, *90*, 2555.

[60] S. Caicedo-Dávila, R. R. Gunder, J. A. Márquez, S. Levcenco, K. Schwarzburg, T. Unold, D. Abou-Ras, S. Caicedo-Davila, R. R. Gunder, J. A. Marquez, S. Levcenco, K. Schwarzburg, T. Unold, D. Abou-Ras, *J. Phys. Chem. C* **2020**, *124*, 19514.

[61] T. Schmidt, K. Lischka, W. Zulehner, *Phys. Rev. B* **1992**, *45*, 8989.

[62] A. Zubiaga, J. A. García, F. Plazaola, V. Muñoz-Sanjosé, C. Martínez-Tomás, *Phys. Rev. B* **2003**, *68*, 245202.

[63] C. Spindler, T. Galvani, L. Wirtz, G. Rey, S. Siebentritt, *J. Appl. Phys.* **2019**, *126*, 175703.

[64] Y. Kajino, S. Otake, T. Yamada, K. Kojima, T. Nakamura, A. Wakamiya, Y. Kanemitsu, Y. Yamada, *Phys. Rev.* **2022**, *6*, L043001.

[65] P. Villars, K. Cenzual, *Cs4PbBr6 Crystal Structure: Datasheet from "PAULING FILE Multinaries Edition – 2022" in SpringerMaterials*, Springer-Verlag Berlin Heidelberg & Material Phases Data System (MPDS), Switzerland & National Institute for Materials Science (NIMS), Japan.

[66] C. K. Moller, *Nature* **1958**, *182*, 1436.

[67] *CsPb2Br5 (T = 300 K) crystal structure: Datasheet from "PAULING FILE multinaries edition – 2022" in SpringerMaterials* (Eds.: P. Villars, K. Cenzual), Springer-Verlag Berlin Heidelberg & Material Phases Data System (MPDS), Switzerland & National Institute for Materials Science (NIMS), Japan https://www.materials.springer.com/isp/crystallographic/docs/sd_1533100.

[68] L. Bányai, S. W. Koch, *Semiconductor Quantum Dots*, Vol. 2, World Scientific, Singapore **1993**.

[69] D. Fröhlich, K. Heidrich, H. Künzel, G. Trendel, J. Treusch, *J. Lumin.* **1979**, *18–19*, 385.

[70] M. Sebastian, J. A. Peters, C. C. Stoumpos, J. Im, S. S. Kostina, Z. Liu, M. G. Kanatzidis, A. J. Freeman, B. W. Wessels, *Phys. Rev. B: Condens. Matter Mater. Phys.* **2015**, *92*, 235210.

[71] L. Protesescu, S. Yakunin, M. I. Bodnarchuk, F. Krieg, R. Caputo, C. H. Hendon, R. X. Yang, A. Walsh, M. V. Kovalenko, *Nano Lett.* **2015**, *15*, 3692.

[72] G. R. Yettapu, D. Talukdar, S. Sarkar, A. Swarnkar, A. Nag, P. Ghosh, P. Mandal, *Nano Lett.* **2016**, *16*, 4838.

[73] M. Kumagai, T. Takagahara, *Phys. Rev. B* **1989**, *40*, 12359.

[74] P. G. Bolcatto, C. R. Proetto, *Phys. Rev. B: Condens. Matter Mater. Phys.* **1999**, *59*, 12487.

[75] J. L. Movilla, J. Planelles, *Comput. Phys. Commun.* **2005**, *170*, 144.

[76] J. Planelles, *Theor. Chem. Acc.* **2017**, *136*, 81.

[77] F. Rajadell, J. I. Climente, J. Planelles, *Phys. Rev. B* **2017**, *96*, 035307.

[78] L. V. Keldysh, *Pis'ma Zh. Eksp. Teor. Fiz.* **1979**, *29*, 716.

[79] T. Takagahara, *Phys. Rev. B* **1993**, *47*, 4569.

[80] P. G. Bolcatto, C. R. Proetto, *J. Phys. Condens. Matter* **2001**, *13*, 319.

[81] F. Rajadell, J. L. Movilla, M. Royo, J. Planelles, *Phys. Rev. B: Condens. Matter Mater. Phys* **2007**, *76*, 115312.

[82] B. Kang, K. Biswas, *J. Phys. Chem. Lett.* **2018**, *9*, 830.

[83] G. Hu, W. Qin, M. Liu, X. Ren, X. Wu, L. Yang, S. Yin, *J. Mater. Chem. C* **2019**, *7*, 4733.

[84] Q. Zhang, X. Sun, W. Zheng, Q. Wan, M. Liu, X. Liao, T. Hagio, R. Ichino, L. Kong, H. Wang, L. Li, *Chem. Mater.* **2021**, *33*, 3575.

[85] Z.-P. Huang, B. Ma, H. Wang, N. Li, R.-T. Liu, Z.-Q. Zhang, X.-D. Zhang, J.-H. Zhao, P.-Z. Zheng, Q. Wang, H.-L. Zhang, *J. Phys. Chem. Lett.* **2020**, *11*, 6007.

[86] L. Ding, B. Borjigin, Y. Li, X. Yang, X. Wang, H. Li, *ACS Appl. Mater. Interfaces* **2021**, *13*, 51161.

[87] S. Cho, S. H. Yun, *Commun. Chem.* **2020**, *3*, 15.

[88] S. Datta, *Quantum Transport: Atom to Transistor*, Cambridge University Press, Cambridge **2005**.

[89] P. C. Sercel, J. L. Lyons, N. Bernstein, A. L. Efros, *J. Chem. Phys.* **2019**, *151*, 234106.

[90] P. C. Sercel, J. L. Lyons, D. Wickramaratne, R. Vaxenburg, N. Bernstein, A. L. Efros, *Nano Lett.* **2019**, *19*, 4068.

[91] A. Ghribi, R. Ben Aich, K. Boujdaria, T. Barisien, L. Legrand, M. Chamarro, C. Testelin, *Nanomaterials* **2021**, *11*, 3054.

[92] M. Nikl, E. Mihokova, K. Nitsch, *Solid State Commun.* **1992**, *84*, 1089.

[93] S. Kondo, K. Amaya, S. Higuchi, T. Saito, H. Asada, M. Ishikane, *Solid State Commun.* **2001**, *120*, 141.

[94] S. Kondo, A. Masaki, T. Saito, H. Asada, *Solid State Commun.* **2002**, *124*, 211.